Ultrafast Response/Recovery and High Selectivity of H_2S Gas Sensor Based on α-Fe_2O_3 Nano-Ellipsoids from One-Step Hydrothermal Synthesis

Zhonglin Wu[1], Zhijie Li[1*], Hao Li[1], Mengxuan Sun[1], Shaobo Han[1], Chao Cai[2], Wenzhong Shen[3], YongQing Fu[4*]

[1]School of Physics, University of Electronic Science and Technology of China, Chengdu, 610054, China

[2]Institute of Fundamental and Frontier Sciences, University of Electronic Science and Technology of China, Chengdu, 610054, China

[3]State Key Laboratory of Coal Conversion, Institute of Coal Chemistry, Chinese Academy of Science, Taiyuan, 030001, China

[4]Faculty of Engineering and Environment, Northumbria University, Newcastle Upon Tyne, NE1 8ST, UK

Keywords*:* α-Fe_2O_3; Nano-ellipsoid; Hydrothermal; Hydrogen sulfide; Gas sensors

Zhijie Li (**Corresponding Author**): ORCID: 0000-0001-9870-9939;

*E-mail: zhijieli@uestc.edu.cn; TEL: +86 02883202160

YongQing (Richard) Fu (**Corresponding Author**): ORCID: 0000-0001-9797-4036;

*E-mail: Richard.fu@northumbria.ac.uk; TEL: +44 (0)191 2274662

Abstract

Ultrafast response/recovery and high selectivity of gas sensors are critical for real-time and online monitoring of hazardous gases. In this work, α-Fe_2O_3 nano-ellipsoids were synthesized using a facile one-step hydrothermal method and investigated as highly sensitive H_2S sensing materials. The nano-ellipsoids have an average long axis diameter of 275 nm and an average short axis diameter of 125 nm. H_2S gas sensors fabricated using the α-Fe_2O_3 nano-ellipsoids showed excellent H_2S sensing performance at an optimum working temperature of 260 ℃. The response and recovery times were 0.8 s/2.2 s for H_2S gas with a concentration of 50 ppm, which are much faster than those of H_2S gas sensors reported in literature. The α-Fe_2O_3 nano-ellipsoid based sensors also showed a high selectivity to H_2S compared to other commonly investigated gases including NH_3, CO, NO_2, H_2, CH_2Cl_2 and ethanol. In addition, the sensors exhibited high response values to different concentrations of H_2S with a detection limit as low as 100 ppb, as well as excellent repeatability and long-term stability.

1. Introduction

Hydrogen sulfide (H_2S), one of the highly toxic gases, is widely existed in petroleum industry, natural gas and biological decomposition of organic materials and extensively used in many industrial processes. Leakage of H_2S gas will impose tremendous risks on environment and human health even at a very low concentration. Therefore, rapid and selective detection of H_2S gas is of great importance.[1] In recent years, many types of H_2S gas sensors have been developed, such as resistive sensor,[2] electrochemical sensor [3] and surface acoustic wave sensor.[4] Among these, the resistive sensor based on semiconducting metal oxide nanostructures attracts great attention due to its facile fabrication process and excellent sensing performance.[5]

Various semiconducting metal oxide nanostructures[6] have been explored to detect H_2S gas, including ZnO,[7] CeO_2,[8] WO_3,[9-10] CuO,[11] MoO_3,[12] NiO,[13] SnO_2,[14] In_2O_3[15] and α-Fe_2O_3.[16] Among them, the α-Fe_2O_3 nanomaterials are nontoxic, chemically stable and low cost, which are good sensing materials to detect ethanol,[17] acetone,[18]

trimethylamine,[19] NH_3[20] and H_2S.[21] It was reported that α-Fe_2O_3 nanomaterials exhibit good sensing performance for H_2S.[16] It is well known that the size, morphology and porosity of α-Fe_2O_3 nanomaterials significantly affect their gas sensing properties, such as sensitivity, response/recovery times (t_{res}/t_{rec}), selectivity and stability. Therefore, great effort has been made to prepare different α-Fe_2O_3 nanostructures to improve the H_2S gas sensing performance, such as flute-like porous nanorods,[22] micro-ellipsoids,[21] sheaf-like architectures,[17] hollow urchin-like spheres[23] and microcubes[24], etc. The sensing properties of H_2S gas sensors based on different Fe_2O_3 nanostructures reported in literature are summarized in Table 1. It can be found that high response values and ppb level detection limits have been achieved using some Fe_2O_3 nanostructures. However, the response/recovery speeds of these reported H_2S gas sensors based on these α-Fe_2O_3 nanostructures are not fast enough to timely trigger the alarm. In addition, many of these H_2S gas sensors do not show a good selectivity to H_2S gas.[19] For example, although the porous α-Fe_2O_3 exhibited fast responses/recovery speeds at 250 °C, there were no significant difference in the response values toward H_2S and ethanol.[25]

Table 1 Sensing properties of H_2S gas sensors based on different Fe_2O_3 nanostructures

Materials	Working Temp.	Con. (ppm)	Response	t_{res}/t_{rec}	Detection Limit	Ref.
Fe_2O_3 nanoboxes	50	5	2.58	806 s/1100 s	250 ppb	26
Porous α-Fe_2O_3	25	0.05	1.08	250 s/200 s	50 ppb	27
Fe_2O_3 film	250	100	5	64 s/670 s	1 ppm	28
α-Fe_2O_3 micro-ellipsoids	350	100	11.7	78 s/15 s	500 ppb	21
α-Fe_2O_3 nanochains	285	5	4.5	10 s/60 s	1 ppm	29
α-Fe_2O_3 nanosheets	135	5	5.8	10 s/45 s	1 ppm	30
Porous α-Fe_2O_3	250	50	1.6	5 s/10 s	1 ppm	25
Au/Fe_2O_3 thin film	250	10	5.23	80 s/180 s	1 ppm	31
Ag/α-Fe_2O_3 nanoparticles	160	100	220	42 s/26 s	-	32
Pt/α-Fe_2O_3 nanoparticles	150	100	300	100 s/180 s	10 ppm	33
Fe_2O_3/WO_3 nanocrystals	150	5	120	60 s/240 s	500 ppb	34
Fe_2O_3/NiO nanoparticles	200	10	8	100 s/20 s	1 ppm	35

In order to enhance the H_2S gas sensing performance, modifications of the α-Fe_2O_3 nanomaterials using noble metals have been widely reported. For examples, Wang et al.[32] prepared a gas sensor made of Ag modified α-Fe_2O_3 nanoparticles, which showed a high response value of 220 and fast response/recovery times of 42 s /26 s toward 100 ppm H_2S and a good selectivity at 160 ºC. Balouria et al.[31] reported that Au modified α-Fe_2O_3 film achieved the response/recovery times of 80 s/180 s to 10 ppm H_2S and a good H_2S selectivity compared to gases of C_2H_5OH, CO, NH_3, CO_2, NO and Cl_2 at 250 ºC. Although the response values, selectivity and response/recovery speeds of these α-Fe_2O_3 based H_2S gas sensors have been remarkably improved by modification using noble metal nanoparticles, the response/recovery times are still mostly longer than 40 s. Therefore, it is still a critical challenge to optimize the α-Fe_2O_3 nanostructures for achieving the best sensing performance to H_2S gas with fast response/recovery speeds, high sensitivity and good selectivity.

Nanocrystals of α-Fe_2O_3 are usually prepared using multiple processes. For example, the precursor of iron hydroxide is often initially prepared using a hydrothermal method,[16] a sol–gel method[36] or an electrospinning method,[37] and then the iron hydroxide is calcined to obtain α-Fe_2O_3 nanocrystals. The increases of nanocrystal sizes are often observed during the calcining process, which will influence the sensing performance. However, there are few reports for using one-step synthesis method to produce the α-Fe_2O_3 nanocrystals.

In this work, α-Fe_2O_3 nano-ellipsoids were directly synthesized using a facile one-step hydrothermal method. The H_2S gas sensors based on these α-Fe_2O_3 nano-ellipsoids exhibit not only high response values, but also ultrafast response/recovery speeds and good selectivity to H_2S gas.

2. Experimental Section

2.1 Synthesis and characterization of α-Fe_2O_3 nano-ellipsoids

Iron nitrate nonahydrate ($Fe(NO_3)_3 \cdot 9H_2O$), sodium nitrate ($NaNO_3$), sodium dodecyl sulfate (SDS), ethanolamine, urea, ethyl alcohol and n, n-dimethylformamide (DMF)

were obtained from Sinopharm Chemical Reagents Limited, Shanghai, China, all with the analytical purity.

In a typical hydrothermal process, 1.616 g of $Fe(NO_3)_3 \cdot 9H_2O$ and 2.0 g of urea were dissolved into a mixed solution which contained 20 mL of distilled water, 9 mL of ethyl alcohol and 1 mL of ethanolamine under a continuous magnetic stirring. After stirring for 10 min, 0.5 g $NaNO_3$ and 0.5 g SDS were successively added into the above solution to form a homogeneous solution. Then, 5 mL of DMF was added drop by drop into the above solution under a magnetic stirring and the solution was maintained under an ultrasonic agitation for 30 min. The hydrothermal reaction was maintained at 120 ºC for 20 hrs in a 50 mL Teflon-lined autoclave in an air oven. After that, the red-brown precipitate in the autoclave was washed using a mix solution of deionized H_2O and anhydrous ethyl alcohol for four times. Finally, it were dried at 60 ºC for 10 hrs to obtain red-brown α-Fe_2O_3 nano-ellipsoids.

Crystalline structure of the α-Fe_2O_3 nano-ellipsoids was characterized using X-ray diffraction (XRD, D/MAX-2500) with Cu Kα radiation. Their morphologies were observed using a scanning electron microscope (SEM, Inspect F50, USA) and a transmission electron microscope (TEM, JEM-2200FS, Japan) attached with selected-area electron diffraction (SAED). Chemical binding information of the α-Fe_2O_3 nano-ellipsoids was characterized using an X-ray photoelectron spectroscope (XPS, Thermo Fisher Scientific) with Al Kα radiation. The specific surface area was measured using the N_2 physisorption apparatus (JW-BK122W, JWGB SCI. TECH.) and the data was calculated using the Brunauer-Emmett-Teller (BET) method. Fourier transform infrared (FT-IR) spectrum was recorded using an FT-IR transmittance spectrometer (FT-IR, Nicolet 6700, USA).

2.2 Sensor Fabrication and Measurement

The gas sensors were made on the alumina ceramic tubes, and Ni-Cr heating resistors were used to control the working temperature. The α-Fe_2O_3 nano-ellipsoids were dispersed into ethanol, and then dip-coated on the surface of the tube to form a uniform sensing layer. The thickness of the α-Fe_2O_3 nano-ellipsoid layer was about 20 μm. This tube with the layer of α-Fe_2O_3 nano-ellipsoids was heated at 500 ºC for 2 hrs in air. The

detailed configuration of the gas sensor device has been previously reported.[11] The sensor devices were placed in a chamber of airproof black box (with a volume of 2 liters) for the evaluation of gas sensing performance. The H_2S gas was injected into the black box using a microinjector to achieve the required concentration. The electrical resistances of the sensor were measured using a source meter (Keithley 2400), and a computer with a suitable Lab View interface was used to handle the data acquisition. During the measurement, the working voltage was set as 1 V. The response value is defined using the following equation: $S = R_a/R_g$ (R_a and R_g are the sensors' resistance readings in air and the target gases, respectively). The selectivity coefficient (S_{AB}) of gas A to gas B is defined as S_A/S_B, where S_A and S_B are the response values to H_2S gas and to other gases (e.g., C_2H_5OH, CO, NO_2, H_2, CH_2Cl_2, NH_3 in this study), respectively. The response times (t_{res}) is defined as the time at which the response value reaches 90% of its maximum one after the injection of H_2S, while the recovery times (t_{rec}) is defined as the time at which the response value is decreased to its 10% of its maximum one after the H_2S was replaced by air.[38]

3. Results and discussion

3.1 Characterization of the α-Fe_2O_3 nano-ellipsoids

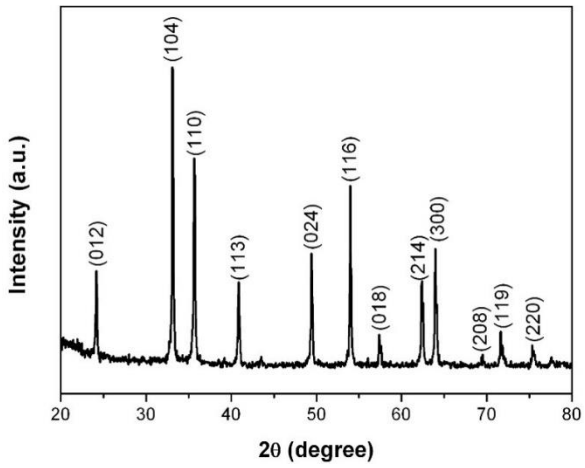

Fig. 1 XRD spectrum of the α-Fe_2O_3 nano-ellipsoids.

XRD spectrum of the α-Fe_2O_3 nano-ellipsoids is shown in Fig. 1. For the α-Fe_2O_3 nano-ellipsoids obtained from the hydrothermal reaction, all the diffraction peaks in the

spectrum are corresponding to (012), (104), (110), (113), (024), (116), (018), (214), (300), (208), (119) and (220) crystal planes of the rhombohedral phase of α-Fe_2O_3 crystalline structure (JCPDS No. 33-0664), with lattice parameters of a = b = 5.036Å, c = 13.747Å. No peaks associated with other phases are observed, suggesting that the as-synthesized powders after the hydrothermal reaction are pure α-Fe_2O_3 crystals. This indicates that the α-Fe_2O_3 nanocrystals with a rhombohedral crystal structure can be directly prepared using the one-step hydrothermal process in this study.

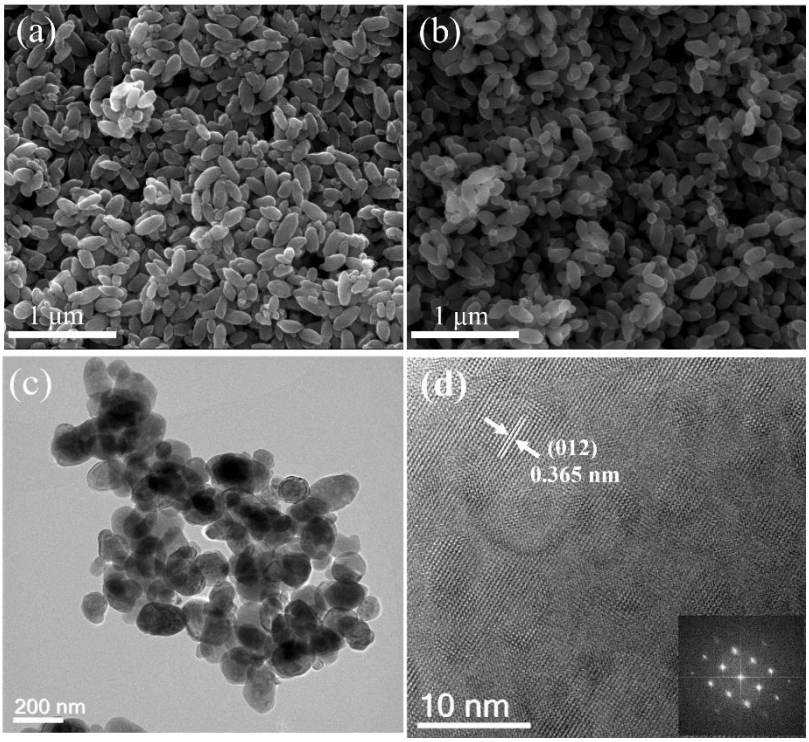

Fig. 2 (a) SEM image of α-Fe_2O_3 nano-ellipsoids, (b) SEM images of α-Fe_2O_3 nano-ellipsoids after calcination at 500 ºC, (c) TEM image of α-Fe_2O_3 nano-ellipsoids after the calcination process at 500 ºC and (d) the corresponding HRTEM image. Inset in (d) shows the SAED pattern of α-Fe_2O_3 nano-ellipsoids.

As can be seen from the SEM image shown in Fig. 2a, the morphology of as-prepared α-Fe_2O_3 nanocrystals after the hydrothermal process are nano-ellipsoids. These α-Fe_2O_3 nano-ellipsoids have an average long axis diameter of 275 nm and an average short axis diameter of 125 nm. No other types of morphologies are observed. After these nano-ellipsoids were annealed at 500 ºC for 2hrs, the morphology and size of α-Fe_2O_3 nano-

ellipsoids are not significantly changed as shown in the SEM image in Fig 2b, indicating that the α-Fe_2O_3 nano-ellipsoids have good stability when annealed at high temperature. In addition, it can be found from the TEM image (see Fig. 2c) that the α-Fe_2O_3 nano-ellipsoids after calcination at 500 ºC have smooth surfaces without any apparent pores. The smooth surface of the annealed α-Fe_2O_3 nano-ellipsoids can facilitate fast absorption and desorption of H_2S gas molecules, which is beneficial to the fast response and recovery of gas sensor. As observed in Fig. 2d, the lattice fringe analysis shows that the interplanar distance of 0.365 nm is corresponding to (012) planes of α-Fe_2O_3. The SAED pattern shown in the inset of Fig. 2d demonstrates that the α-Fe_2O_3 nano-ellipsoids are crystalline in nature. The BET surface area of the α-Fe_2O_3 nano-ellipsoids obtained by the N_2 physisorption is 12.09 m^2/g.

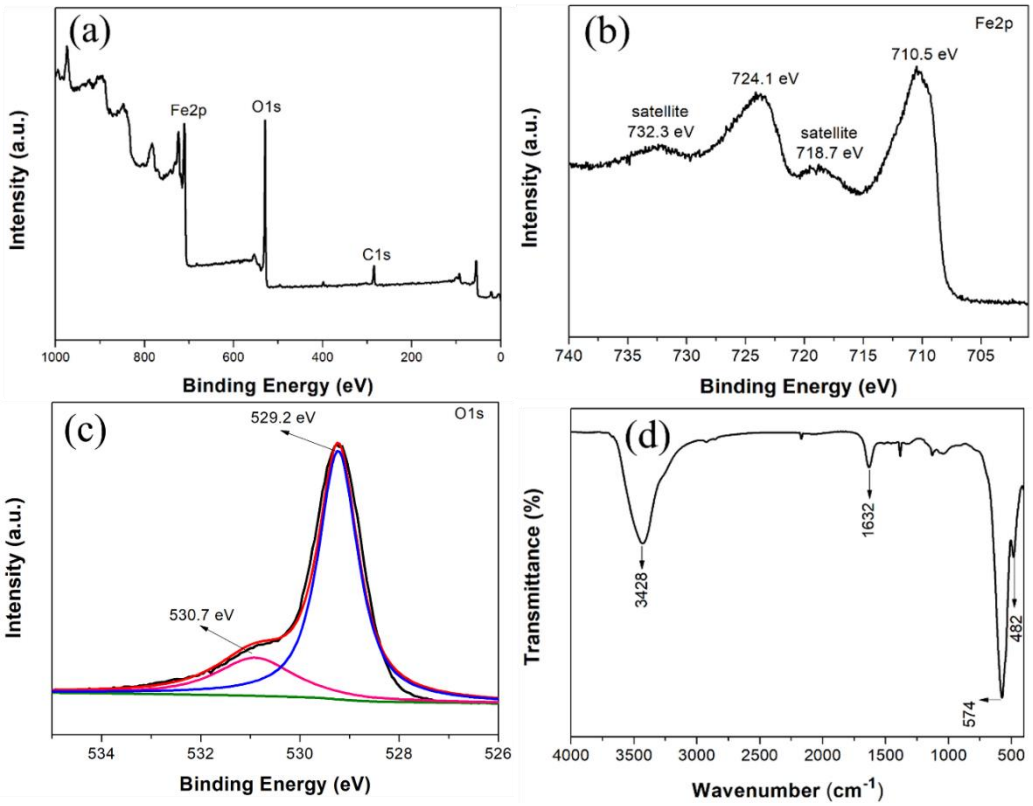

Fig. 3. (a) XPS survey spectrum, (b) Fe 2p and (c) O 1s high-resolution spectra of the α-Fe_2O_3 nano-ellipsoids, (d) FT-IR spectrum of the α-Fe_2O_3 nano-ellipsoids.

XPS survey spectrum of the α-Fe_2O_3 nano-ellipsoids is shown in Fig. 3a. It reveals the presence of Fe, O, and C elements. The binding energy peaks at 724.1 and 710.5 eV

and their corresponding satellite peak at 732.3 and 718.7 eV in the Fe 2p high-resolution XPS spectrum in Fig. 3(b) are attributed to Fe $2p_{1/2}$ and Fe $2p_{3/2}$, respectively,[19] which proves that the chemical state of iron element is Fe^{3+}.[27, 33] Two obvious peaks can be observed in the O 1s high-resolution XPS spectrum as shown in Fig. 3(c), which have the binding energy values of 529.2 and 530.7 eV. The peak located at 529.2 eV is associated with the lattice oxygen atoms in α-Fe_2O_3, and the peak located at 530.7 eV is linked with the chemisorbed oxygen species on the surface of α-Fe_2O_3 nano-ellipsoids. The large peak area of chemisorbed oxygen species in Fig. 3(c) means that there are many chemisorbed oxygen species on the surfaces of α-Fe_2O_3 nano-ellipsoids.[33]

Fig. 3 (d) shows the FT-IR spectrum of the α-Fe_2O_3 nano-ellipsoids. The peaks at 482 cm^{-1} and 574 cm^{-1} are corresponding to the Fe-O vibration modes of α-Fe_2O_3. The peak at 3428 cm^{-1} can be assigned to O-H stretching vibration mode of the absorbed water molecules, and that at 1632 cm^{-1} can be assigned to O-H bending vibration of absorbed water.

3.2 **Gas-sensing properties**

Fig. 4(a) shows typical current-voltage (I-V) curves measured with the two neighboring platinum electrodes bridged by the α-Fe_2O_3 nano-ellipsoids layer at working temperatures from 100 ºC to 340 ºC. All the current values are increased linearly with the applied bias voltage increased from -10 V to 10 V. Such a linear behavior reveals a good ohmic contact formed between the α-Fe_2O_3 nano-ellipsoid layer and Au electrodes. Moreover, when the working temperature is increased, the conductivity of the α-Fe_2O_3 nano-ellipsoid layer is increased, which is consistent with the conduction behavior of a standard semiconductor.

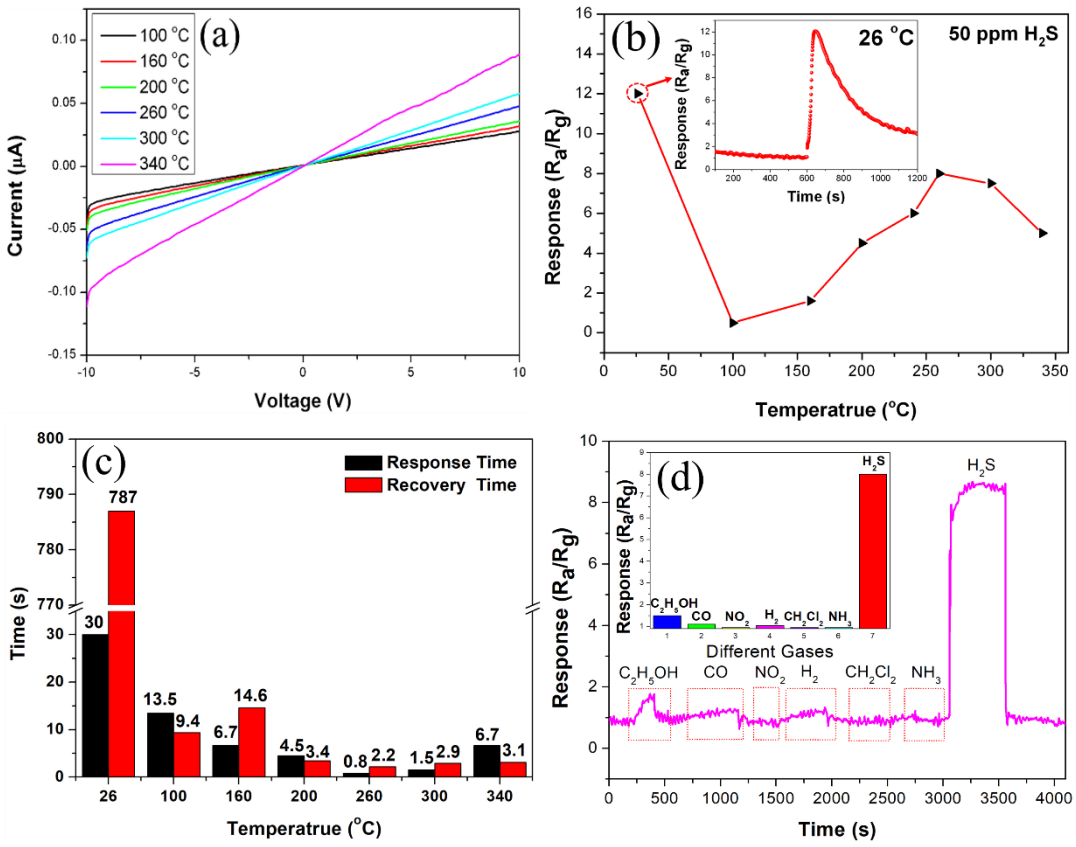

Fig. 4 (a) I-V curves of the α-Fe_2O_3 nano-ellipsoids based sensor device at different working temperatures. (b) Response values of the sensor to H_2S (50 ppm) at different working temperatures (the inset in b is the response/recovery curves of 50 ppm H_2S at 26 °C). (c) the corresponding response/recovery times from 100 °C to 340 °C (d) response/recovery curves of the sensor to various gases at a fixed concentration of 50 ppm at 260 °C (the inset in (d) is the response histogram).

The working temperature affects the adsorption/desorption rates of oxygen molecules and target gas molecules on the surface of metal oxides, and thus affects the sensitivity of metal oxide based gas sensor. The response values of the α-Fe_2O_3 nano-ellipsoids based sensor to 50 ppm H_2S have been tested at various working temperatures from 26 °C to 340 °C, and the obtained data are shown in Fig. 4 (b). The gas sensor shows the highest response value of 12.0 at the room temperature of 26 °C. However, as shown in Fig. 4 (b), the long response time (30 s) and recovery time (~ 787 s) of the sensor for sensing 50 ppm H_2S make it unsuitable for real-time application for the H_2S detection operated at room temperature. Whereas when the sensor was operated at

different working temperature from 100 ºC to 340 ºC, all the obtained response/recovery times are less than 15 s as shown in Fig 4 (c). With the increase of working temperature from 100 ºC to 260 ºC, the responses values are increased as shown in Fig. 4(b). However, they are then slowly decreased with the further increase of working temperature. The response value of the α-Fe_2O_3 nano-ellipsoids based sensor achieves a high value of 8.0 at 260 ºC, which is higher than many reported values for sensors made of pure α-Fe_2O_3. For example, the response values of the sensors made of porous α-Fe_2O_3 [25] and Fe_2O_3 film [28] were 1.6 to 50 ppm of H_2S and 5 to 100 ppm H_2S operated at 250 ºC, respectively. Taking into accounts of both response/recovery times and sensitivity response, the optimum working temperature for this study is 260 ºC for the H_2S gas sensor based on α-Fe_2O_3 nano-ellipsoids.

The high response values of the α-Fe_2O_3 nano-ellipsoids based sensor when operated at room temperature can be explained as follows. Besides the chemical reactions between H_2S molecules and chemisorption oxygen ions, the formation of iron sulphides (i.e. Fe_2S_3) on the surfaces of α-Fe_2O_3 nano-ellipsoids due to the reaction between H_2S and Fe_2O_3 is another important factor to enhance the response values of the sensor.[27] It was reported that the H_2S molecules can generate ions of S^{2-} and H^+ on the surfaces of Fe_2O_3 to form iron sulphides, even at room temperature.[39] Therefore, iron sulphides can be easily formed onto the surfaces of α-Fe_2O_3 nano-ellipsoids, which results in a much higher response value than those operated at a much higher working temperatures. However, the formation rate of these iron sulphides is slow at room temperature, which means that the longer response time is needed. For example, Huang et al reported that the porous-Fe_2O_3 based H_2S gas sensor showed the highest sensitivity of 38.4 but with long response/recovery times of about180/3700 s when sensing 100 ppm H_2S operated at room temperature.[27]

When the working temperature is increased to above 100 ºC, the chemical reactions between H_2S molecules and chemisorption oxygen ions becomes dominant.[39] More active oxygen ions can form and the chemical activation potentials of sensing materials have been increased with the increase of working temperature, all of which can enhance the response values of the gas sensor. However, at a very high working temperature, the

adsorbed gas molecules can be quickly released from the surface of materials before the chemical reaction happens. Therefore, with the further increase of the working temperature, the quantities of the adsorbed H_2S molecules are decreased significantly, thus resulting in the decreased responses.[40] Clearly, there is an optimum working temperature for these resistive H_2S gas sensors, such as those based on Fe_2O_3 film,[28] α-Fe_2O_3 micro-ellipsoids,[21] α-Fe_2O_3 nanochains[29] and Au/Fe_2O_3 thin films [31], whose optimum working temperatures were reported to be 250, 350, 285 and 250 °C, respectively.

Good selectivity is another important requirement of gas sensors in order to avoid the interference from the other gases during gas sensing. The response/recovery curves of the α-Fe_2O_3 nano-ellipsoid based gas sensor to different gases (including C_2H_5OH, CO, NO_2, H_2, CH_2Cl_2, NH_3) were measured at the same concentration of 50 ppm at 260 °C and these obtained results are shown in Fig. 4(d). It can be found that the gas sensor shows insignificant responses toward NO_2, CH_2Cl_2 and NH_3, and the response values toward C_2H_5OH, CO and H_2 are also very small, e.g., 1.5, 1.1 and 1.05, respectively. The response value of 8.0 towards H_2S for this gas sensor is remarkable higher than the values towards other types of gases. The selective coefficients (S_{AB}, which is defined as the ratio of response values of gas sensor for H_2S and other gases) are 5.3, 7.0 and 7.6 for C_2H_5OH, CO and H_2, respectively. Generally, when the selective coefficient of a gas sensor is higher than 3, this gas sensor is regarded as having a good selectivity. For examples, the H_2S gas sensors made of porous $ZnFe_2O_4$ nanosheets[41] and porous ZnO thin film[42] showed H_2S selective coefficients of 5.3 and 4.1 to ethanol, respectively. The nanocrystalline ZnO thin films based H_2S gas sensor[43] showed the H_2S selective coefficient of 3.48 to NH_3 and 2.92 to ethanol. All these above-mentioned H_2S gas sensors are regarded to have a good selectivity to H_2S. For the α-Fe_2O_3 nano-ellipsoids based H_2S gas sensor in this study, its high selective coefficient value reveals its excellent H_2S selectivity.

Various factors influence the selectivity of gas sensor. Firstly, the different responses of gas sensor toward different gases are mainly due to the chemical properties of gas molecules. The bond dissociation energy of H-S in H_2S molecules is only 381 kJ/mol,

which is smaller than those of other interfering gases.[44] Consequently, compared to those of the other gases, the H-S bonds in H_2S molecules can be easily broken due to the chemisorbed oxide ions on the surface of α-Fe_2O_3 nano-ellipsoids, thus achieving a high response. On the other hand, the higher response of the sensor to H_2S than those to the other gases is also attributed to the formation of iron sulphides on the surface of α-Fe_2O_3 nano-ellipsoids, which can improve the response due to its higher conductance value than that of the α-Fe_2O_3.[42] Whereas there is no such effect when the sensor is used for the other types of gases. Therefore, the gas sensor based on α-Fe_2O_3 nano-ellipsoids based H_2S gas sensor displays a good selectivity to H_2S gas.

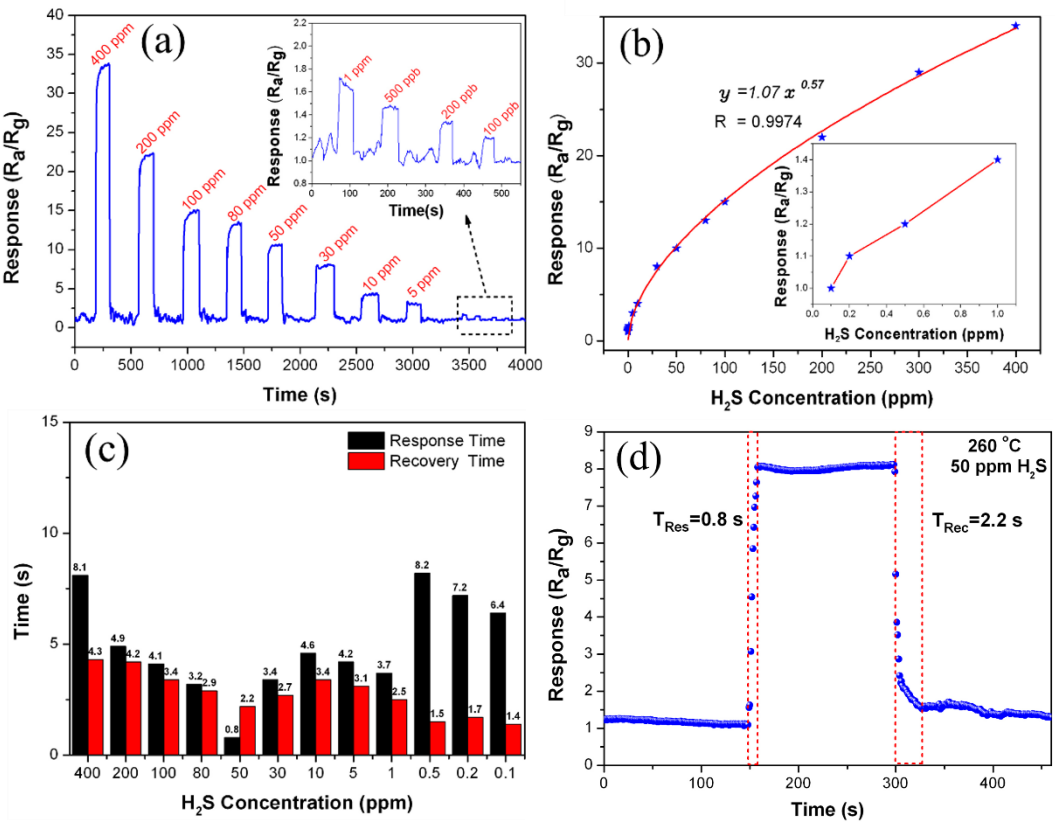

Fig. 5 (a) Response/recovery curves of α-Fe_2O_3 nano-ellipsoids based sensors for various H_2S concentrations (100 ppb~400 ppm) at 260 ºC, (b) the corresponding response values and (c) the corresponding response/recovery times, (d) the high-resolution response/recovery curve toward 50 ppm H_2S at 260 ºC.

Fig. 5(a) shows the response/recovery curves of the α-Fe_2O_3 nano-ellipsoid sensors toward various H_2S concentrations (100 ppb~400 ppm) operated at 260 ºC, and the

corresponding response values are shown in Fig. 5 (b). For all different concentrations of H_2S, this gas sensor can be fully recovered (e.g., returning back to the baseline) after the H_2S gas is quickly replaced with air, which indicates that the sensor made of the α-Fe_2O_3 nano-ellipsoids has an excellent reversibility. It also show high responses as can be seen in Fig. 5(b), e.g., the response is as high as 33.1 for detecting 400 ppm H_2S. Even when the H_2S concentration is as low as 100 ppb, the sensor still exhibits obvious response/recovery phenomena with a response of 1.2, indicating that the sensor can detect a low H_2S concentration down to ppb-level.

Furthermore, the response value (S) and concentration of H_2S (C_{H2S}) are found to have a power law function relation (as listed in equation (1)) with a good correlation coefficient (R = 0.9974). This is beneficial for precisely detecting the concentrations of H_2S gas.

$$S = 1.07C_{H2S}^{0.57} \qquad (R = 0.9974) \qquad (1)$$

The fast response/recovery speeds play a vital role for real-time detection of the toxic gases. For all response/recovery curves of the sensors based on the α-Fe_2O_3 nano-ellipsoids to various H_2S concentrations, the resistance value of the sensor is decreased sharply after injection of H_2S gas, whereas it quickly returns to the baseline quickly after the release of H_2S. This indicates that the H_2S gas sensor has very fast response/recovery speeds. The obtained response/recovery times are shown in Fig. 5 (c), and all the response times are less than 9 s and all the recovery times are less than 5 s. When the H_2S concentrations are increased from 1 ppm to 200 ppm, the response/recovery times are all less than 5 s. Fig. 5 (d) shows the response/recovery curve toward 50 ppm of H_2S with a sampling interval of 0.1 s. It is found that the response and recovery times to 50 ppm H_2S are only 0.8 s and 2.2 s respectively, showing an ultra-fast response/recovery behavior of the sensor.

Compared with the other reported Fe_2O_3 based H_2S gas sensors listed in Table 1, it is worthwhile to note that the α-Fe_2O_3 nano-ellipsoid based H_2S gas sensor developed in this study exhibits much faster response/recovery speeds (for examples, compared to those based on Fe_2O_3 nanostructures,[21, 25-30] noble metal modified Fe_2O_3 [31-33] and hybrid Fe_2O_3 nanostructures [34-35]). Furthermore, compared with other semiconducting metals

oxides based H_2S gas sensors reported in the literature (some of them are listed in Table 2), the response/recovery speeds of the H_2S gas sensor developed in this study are the fastest values as far as we have searched in the literature. For examples, the H_2S gas sensors based on various nanostructures of Co_3O_4,[45] SnO_2,[44, 46,] α-MoO_3,[12, 47] ZnO,[48-50] WO_3 [51] and CuO [52-55, 50, 56,] all showed much longer response/recovery times than those of the α-Fe_2O_3 nano-ellipsoids reported in this study.

Table 2 Sensing properties of H_2S gas sensors based on other semiconducting metal oxide nanomaterials.

Materials	Working Temp.(°C)	Con. (ppm)	Response	t_{res}/t_{rec}	Detection Limit	Ref.
α-MoO_3	177	100	225	15 s/23 s	1 ppm	[12]
CuO	325	0.01	1.3	810 s/1080 s	100 ppb	[52]
CuO	25	1	2.1	240 s/1341 s	100 ppb	[53]
CuO	30	300	1.3	180 s/150 s	10 ppm	[54]
WO_3	300	2	6.7	~120 s/~300 s	120 ppb	[51]
Co_3O_4	300	100	4	46 s/24 s	1 ppm	[45]
ZnO	25	5	581	500 s/6000 s	0.5 ppm	[48]
ZnO	25	50	113.5	16 s/820 s	10 ppm	[49]
TiO_2	100	10	275	150 s/2500 s	1 ppm	[57]
Pt/SnO_2	300	1	89.3	99 s/111 s	100 ppb	[44]
Pd/CuO	300	20	69.04	700 s/120 s	-	[55]
Fe/SnO_2	225	10	14.5	90 s/98 s	-	[46]
Cd/α-MoO_3	140	50	229	23 s/45 s	5 ppm	[47]
SnO_2/CuO	180	100	25.3	10 s/42 s	10 ppm	[56]
CuO/NiO	260	100	46.7	18 s/29 s	10 ppm	[58]
CuO/ZnO	336	5	13.3	270 s/720 s	5 ppm	[50]
TiO_2/Al_2O_3	650	1000	38.7	390 s/480 s	20 ppm	[59]
α-Fe_2O_3	260	50	8.0	0.8 s/2.2 s	100 ppb	this work

It is well known that α-Fe_2O_3 is an n-type semiconducting metal oxide and the surface chemical reactions between the adsorbed oxygen species and target gases are

responsible for the gas sensing performance. Fig. 6 shows a schematic illustration of H_2S sensing process on the surface of α-Fe_2O_3 nano-ellipsoids. The possible reactions that have taken place on the surfaces of α-Fe_2O_3 nano-ellipsoids are listed as follows:[47]

$$O_{2(ads)} + 2e^- \rightarrow 2O_{(ads)}^- \quad (100 \sim 300\ ^\circ C) \tag{2}$$

$$H_2S + 3O_{(ads)}^- \rightarrow SO_2 + H_2O + 3e^- \tag{3}$$

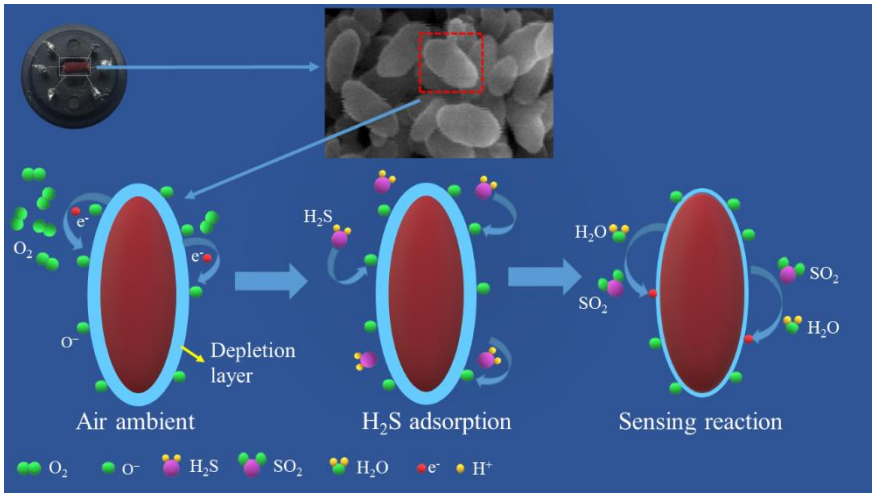

Fig. 6 Schematic illustration of H_2S sensing mechanism on the surface of α-Fe_2O_3 nano-ellipsoids.

In air, the chemisorbed oxygen ions on the surfaces of α-Fe_2O_3 nano-ellipsoids are mainly O^- ions at the working temperature of 260 °C.[60] Oxygen molecules are adsorbed onto the surfaces of α-Fe_2O_3 nano-ellipsoids, and then transfer into O^- ions by gaining electrons from the conductive bands of α-Fe_2O_3 to form O^- ions (as shown in reaction equation (2)). Therefore, an electron depletion layer with a high-resistance state is formed on the surface of α-Fe_2O_3 nano-ellipsoids as shown in Fig. 6. When the α-Fe_2O_3 nano-ellipsoids are exposed to H_2S gas, H_2S molecules react with the chemisorbed oxygen (O^-), as listed in reaction equation (3). The reaction releases electrons to the electron depletion layers and thus reduces the resistance of the α-Fe_2O_3 nano-ellipsoids as shown in Fig. 6.

In addition, the H_2S molecules can react with the lattice oxygen on the surface of the α-Fe_2O_3 nano-ellipsoids to form iron sulphides (Fe_2S_3), based on the reaction equation (4).[28] Fe_2S_3 has a lower band gap than Fe_2O_3, which can cause the increase of surface conductance.[61] When the H_2S gas is replaced with the air, the recovery of Fe_2O_3 from Fe_2S_3 will occur due to the reaction of the Fe_2S_3 with the active oxygen ions of O^- at

the working temperature of 260 ºC as shown in the reaction equation (5).[28, 39]

$$H_2S + Fe_2O_3 \rightarrow Fe_2S_3 + 3H_2O \quad (4)$$

$$Fe_2S_3 + 9O^- \rightarrow Fe_2O_3 + 3SO_2 \quad (5)$$

The excellent H_2S gas sensing performance of the α-Fe_2O_3 nano-ellipsoids based sensor can be attributed to their homogeneous and smooth surface nanostructures, which promote the rapidly adsorptions of the O_2 and H_2S molecules.

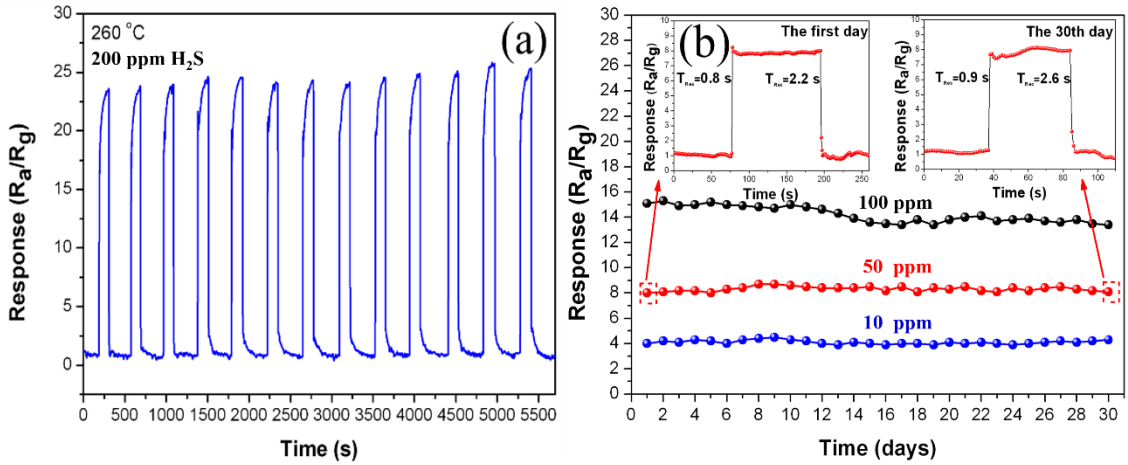

Fig. 7 (a) Repeatability of α-Fe_2O_3 nano-ellipsoids based sensors for 200 ppm H_2S at 260 ℃, (b) long-term stability of α-Fe_2O_3 nano-ellipsoids to H_2S with the concentration of 100 ppm (black), 50 ppm (red) and 10 ppm (blue), respectively.

The repeatability of the gas sensors was further investigated by measuring the 200 ppm of H_2S at the optimum operating temperature of 260 ℃, and the obtained results are shown in Fig. 7 (a). It is found that all the response/recovery curves are repeatable without any significant changes, and the sensor maintains the similar responses and ultrafast response/recovery speeds within 13 cycles, indicating its good repeatability.

In order to prove its long-term stability, the sensor has been tested repeatedly for 30 days. The response values are shown in Fig. 7 (b). In the repeated tests for 30 days, the responses of the sensor toward the H_2S gas with various concentrations (100 ppm, 50 ppm and 10 ppm) only show minor fluctuations within a small range. Moreover, comparing the response/recovery curves of 50 ppm H_2S measured on the first day and the last day as shown in the Fig. 7 (b), the response/recovery curves have not shown apparent differences, and the response/recovery times are 0.8 s/2.2 s and 0.9 s/2.6 s,

respectively. Therefore, the H_2S gas sensor based on α-Fe_2O_3 nano-ellipsoids has shown a good long-term stability.

4. Conclusions

In conclusion, a facile one-step hydrothermal method can be used to prepare the α-Fe_2O_3 nano-ellipsoids. The uniformly formed α-Fe_2O_3 nano-ellipsoids have smooth and dense surfaces. Such α-Fe_2O_3 nano-ellipsoids based gas sensor exhibits excellent H_2S gas sensing performance with fast response/recovery speeds, good selectivity and a low detection limit at an optimum temperature of 260 ℃. Moreover, this sensor shows a good repeatability and stable recycling performance as well as a good long-term stability. Therefore, the α-Fe_2O_3 nano-ellipsoids based gas sensor can be successfully applied in detetion H_2S gas.

Acknowledgments

This work is supported by the Funding supports from UK Engineering Physics and Science Research Council (EPSRC EP/P018998/1), Newton Mobility Grant (IE161019) through Royal Society and NFSC, and Royal academy of Engineering UK-Research Exchange with China and India are also acknowledged.

Conflicts of interest

There are no conflicts to declare.

References

(1) Hao, X.; Ma, C.; Yang, X.; Liu, T.; Wang, B.; Liu, F.; Liang, X.; Yang, C.; Zhu, H.; Lu, G. Ysz-Based Mixed Potential H_2S Sensor Using La_2NiO_4 Sensing Electrode. *Sens. Actuators, B.* **2018,** *255*, 3033-3039.

(2) Deng, J.; Ma, J.; Mei, L.; Tang, Y.; Chen, Y.; Lv, T.; Xu, Z.; Wang, T. Porous Alpha-Fe_2O_3 Nanosphere-Based H_2S Sensor with Fast Response, High Selectivity and Enhanced Sensitivity. *J. Mater. Chem. A.* **2013,** *1*, 12400-12403.

(3) Spilker, B.; Randhahn, J.; Grabow, H.; Beikirch, H.; Jeroschewski, P. New Electrochemical Sensor for the Detection of Hydrogen Sulfide and Other Redox Active Species. *J. Electroanal. Chem.* **2008,** *612*, 121-130.

(4) Fu, Y. Q.; Luo, J. K.; Nguyen, N. T.; Walton, A. J.; Flewitt, A. J.; Zu, X. T.; Li, Y.; McHale, G.;

Matthews, A.; Iborra, E.; Du, H.; Milne, W. I. Advances in Piezoelectric Thin Films for Acoustic Biosensors, Acoustofluidics and Lab-on-Chip Applications. *Prog. Mater. Sci.* **2017,** *89*, 31-91.
(5) Diao, K.; Zhou, M.; Zhang, J.; Tang, Y.; Wang, S.; Cui, X. High Response to H_2S Gas with Facile Synthesized Hierarchical ZnO Microstructures. *Sens. Actuators, B.* **2015,** *219*, 30-37.
(6) Mirzaei, A.; Kim Sang, S.; Kim Hyoun, W. Resistance-Based H_2S Gas Sensors Using Metal Oxide Nanostructures: A Review of Recent Advances. *J. Hazard. Mater.* **2018,** *357*, 314-331.
(7) Deng, J.; Fu, Q.; Luo, W.; Tong, X.; Xiong, J.; Hu, Y.; Zheng, Z. Enhanced H_2S Gas Sensing Properties of Undoped ZnO Nanocrystalline Films from QDs by Low-Temperature Processing. *Sens. Actuators, B.* **2016,** *224*, 153-158.
(8) Li, Z.; Niu, X.; Lin, Z.; Wang, N.; Shen, H.; Liu, W.; Sun, K.; Fu Yong, Q.; Wang, Z. Hydrothermally Synthesized CeO_2 Nanowires for H_2S Sensing at Room Temperature. *J. Alloys Compd.* **2016,** *682*, 647-653.
(9) Li, Y.; Luo, W.; Qin, N.; Dong, J.; Wei, J.; Li, W.; Feng, S.; Chen, J.; Xu, J.; Elzatahry Ahmed, A.; Es-Saheb Mahir, H.; Deng, Y.; Zhao, D. Highly Ordered Mesoporous Tungsten Oxides with a Large Pore Size and Crystalline Framework for H_2S Sensing. *Angew. Chem., Int. Ed.* **2014,** *53*, 9035-9040.
(10) Xiao, B.; Zhao, Q.; Xiao, C.; Yang, T.; Wang, P.; Wang, F.; Chen, X.; Zhang, M. Low-Temperature Solvothermal Synthesis of Hierarchical Flower-Like WO_3 Nanostructures and Their Sensing Properties for H_2S. *CrystEngComm.* **2015,** *17*, 5710-5716.
(11) Li, Z.; Wang, N.; Lin, Z.; Wang, J.; Liu, W.; Sun, K.; Fu Yong, Q.; Wang, Z. Room-Temperature High-Performance H_2S Sensor Based on Porous CuO Nanosheets Prepared by Hydrothermal Method. *ACS Appl. Mater. Interfaces.* **2016,** *8*, 20962-20968.
(12) Zhang, L.; Liu, Z.; Jin, L.; Zhang, B.; Zhang, H.; Zhu, M.; Yang, W. Self-Assembly Gridding Alpha-MoO_3 Nanobelts for Highly Toxic H_2S Gas Sensors. *Sens. Actuators, B.* **2016,** *237*, 350-357.
(13) Yu, T.; Cheng, X.; Zhang, X.; Sui, L.; Xu, Y.; Gao, S.; Zhao, H.; Huo, L. Highly Sensitive H_2S Detection Sensors at Low Temperature Based on Hierarchically Structured NiO Porous Nanowall Arrays. *J. Mater. Chem. A.* **2015,** *3*, 11991-11999.
(14) Hu, J.; Yin, G.; Chen, J.; Ge, M.; Lu, J.; Yang, Z.; He, D. An Olive-Shaped SnO_2 Nanocrystal-Based Low Concentration H_2S Gas Sensor with High Sensitivity and Selectivity. *Phys. Chem. Chem. Phys.* **2015,** *17*, 20537-20542.
(15) Yan, S.; Li, Z.; Li, H.; Wu, Z.; Wang, J.; Shen, W.; Fu, Y. Q. Ultra-Sensitive Room-Temperature H_2S Sensor Using Ag–In_2O_3 Nanorod Composites. *J. Mater. Sci.* **2018,** *53*, 16331-16344.
(16) Li, Z.; Huang, Y.; Zhang, S.; Chen, W.; Kuang, Z.; Ao, D.; Liu, W.; Fu, Y. A Fast Response & Recovery H_2S Gas Sensor Based on Alpha-Fe_2O_3 Nanoparticles with ppb Level Detection Limit. *J. Hazard. Mater.* **2015,** *300*, 167-174.
(17) Sun, P.; Wang, C.; Zhou, X.; Cheng, P.; Shimanoe, K.; Lu, G.; Yamazoe, N. Cu-Doped Alpha-Fe_2O_3 Hierarchical Microcubes: Synthesis and Gas Sensing Properties. *Sens. Actuators, B.* **2014,** *193*, 616-622.
(18) Kim Do, H.; Shim, Y.-S.; Jeon, J.-M.; Jeon Hu, Y.; Park Sung, S.; Kim, Y.-W.; Rim, J.-S.; Lee, J.-H.; Jang Ho, W. Vertically Ordered Hematite Nanotube Array as an Ultrasensitive and Rapid Response Acetone Sensor. *ACS Appl. Mater. Interfaces.* **2014,** *6*, 14779-14784.
(19) Yang, T.; Du, L.; Zhai, C.; Li, Z.; Zhao, Q.; Luo, Y.; Xing, D.; Zhang, M. Ultrafast Response and Recovery Trimethylamine Sensor Based on Alpha-Fe_2O_3 Snowflake-Like Hierarchical Architectures. *J. Alloys Compd.* **2017,** *718*, 396-404.
(20) Li, Y.; Zhao, H.; Ban, H.; Yang, M. Composites of Fe_2O_3 Nanosheets with Polyaniline: Preparation, Gas Sensing Properties and Sensing Mechanism. *Sens. Actuators, B.* **2017,** *245*, 34-43.

(21) Li, Z.; Lin, Z.; Wang, N.; Huang, Y.; Wang, J.; Liu, W.; Fu, Y.; Wang, Z. Facile Synthesis of Alpha-Fe_2O_3 Micro-Ellipsoids by Surfactant-Free Hydrothermal Method for Sub-Ppm Level H_2S Detection. *Mater. Des.* **2016,** *110*, 532-539.
(22) Gou, X.; Wang, G.; Kong, X.; Wexler, D.; Horvat, J.; Yang, J.; Park, J. Flutelike Porous Hematite Nanorods and Branched Nanostructures: Synthesis, Characterisation and Application for Gas-Sensing. *Chem. - Eur. J.* **2008,** *14*, 5996-6002.
(23) Sun, P.; Du, S.; Yang, T.; Li, X.; Liu, F.; Liang, X.; Gao, Y.; Sun, Y.; Lu, G. Controlled Synthesis of Hierarchical Sn-Doped Alpha-Fe_2O_3 with Novel Sheaf-Like Architectures and Their Gas Sensing Properties. *RSC Adv.* **2013,** *3*, 7112-7118.
(24) Shi, G.; Zhang, K.; Zhou, S.; Zhang, Q. Template-Free Synthesis and Gas-Sensing Properties of Hierarchical Alpha-Fe_2O_3 Hollow Urchin-Like Spheres. *Mater. Lett.* **2013,** *107*, 228-230.
(25) Hao, Q.; Li, L.; Yin, X.; Liu, S.; Li, Q.; Wang, T. Anomalous Conductivity-Type Transition Sensing Behaviors of N-Type Porous Alpha-Fe_2O_3 Nanostructures toward H_2S. *Mater. Sci. Eng., B.* **2011,** *176*, 600-605.
(26) Tian, K.; Wang, X.-X.; Yu, Z.-Y.; Li, H.-Y.; Guo, X. Hierarchical and Hollow Fe_2O_3 Nanoboxes Derived from Metal-Organic Frameworks with Excellent Sensitivity to H_2S. *ACS Appl. Mater. Interfaces.* **2017,** *9*, 29669-29676.
(27) Huang, Y.; Chen, W.; Zhang, S.; Kuang, Z.; Ao, D.; Alkurd Nooraldeen, R.; Zhou, W.; Liu, W.; Shen, W.; Li, Z. A High Performance Hydrogen Sulfide Gas Sensor Based on Porous Alpha-Fe_2O_3 Operates at Room-Temperature. *Appl. Surf. Sci.* **2015,** *351*, 1025-1033.
(28) Balouria, V.; Kumar, A.; Samanta, S.; Singh, A.; Debnath, A. K.; Mahajan, A.; Bedi, R. K.; Aswal, D. K.; Gupta, S. K. Nano-Crystalline Fe_2O_3 Thin Films for ppm Level Detection of H_2S. *Sens. Actuators, B.* **2013,** *181*, 471-478.
(29) Ma, J.; Mei, L.; Chen, Y.; Li, Q.; Wang, T.; Xu, Z.; Duan, X.; Zheng, W. Alpha-Fe_2O_3 Nanochains: Ammonium Acetate-Based Ionothermal Synthesis and Ultrasensitive Sensors for Low-Ppm-Level H_2S Gas. *Nanoscale.* **2013,** *5*, 895-898.
(30) Zhang, H.-J.; Meng, F.-N.; Liu, L.-Z.; Chen, Y.-J. Convenient Route for Synthesis of Alpha-Fe_2O_3 and Sensors for H_2S Gas. *J. Alloys Compd.* **2019,** *774*, 1181-1188.
(31) Balouria, V.; Ramgir Niranjan, S.; Singh, A.; Debnath, A. K.; Mahajan, A.; Bedi, R. K.; Aswal, D. K.; Gupta, S. K. Enhanced H_2S Sensing Characteristics of Au Modified Fe_2O_3 Thin Films. *Sens. Actuators, B.* **2015,** *219*, 125-132.
(32) Wang, Y.; Wang, Y.; Cao, J.; Kong, F.; Xia, H.; Zhang, J.; Zhu, B.; Wang, S.; Wu, S. Low-Temperature H_2S Sensors Based on Ag-Doped Alpha-Fe_2O_3 Nanoparticles. *Sens. Actuators, B.* **2008,** *131*, 183-189.
(33) Wang, Y.; Wang, S.; Zhao, Y.; Zhu, B.; Kong, F.; Wang, D.; Wu, S.; Huang, W.; Zhang, S. H_2S Sensing Characteristics of Pt-Doped Alpha-Fe_2O_3 Thick Film Sensors. *Sens. Actuators, B.* **2007,** *125*, 79-84.
(34) Yin, L.; Chen, D.; Feng, M.; Ge, L.; Yang, D.; Song, Z.; Fan, B.; Zhang, R.; Shao, G. Hierarchical Fe_2O_3@WO_3 Nanostructures with Ultrahigh Specific Surface Areas: Microwave-Assisted Synthesis and Enhanced H_2S-Sensing Performance. *RSC Adv.* **2015,** *5*, 328-337.
(35) Li, F.; Chen, Y.; Ma, J. Fe^{3+} Facilitating the Response of NiO Towards H_2S. *RSC Adv.* **2014,** *4*, 14201-14205.
(36) Peng, W.; Zhu, C.; Zhu, S.; Yao, F.; Li, Y.; Zhang, D. Biomimetic Fabrication of Alpha-Fe_2O_3 with Hierarchical Structures as H_2S Sensor. *J. Mater. Sci.* **2013,** *48*, 4336-4344.

(37) Guo, L.; Kou, X.; Ding, M.; Wang, C.; Dong, L.; Zhang, H.; Feng, C.; Sun, Y.; Gao, Y.; Sun, P.; Lu, G. Reduced Graphene Oxide/Alpha-Fe_2O_3 Composite Nanofibers for Application in Gas Sensors. *Sens. Actuators, B.* **2017,** *244*, 233-242.
(38) Jin, W. X.; Ma, S. Y.; Tie, Z. Z.; Jiang, X. H.; Li, W. Q.; Luo, J.; Xu, X. L.; Wang, T. T. Hydrothermal Synthesis of Monodisperse Porous Cube, Cake and Spheroid-Like Alpha-Fe_2O_3 Particles and Their High Gas-Sensing Properties. *Sens. Actuators, B.* **2015,** *220*, 243-254.
(39) Ghosh, S.; Adak, D.; Bhattacharyya, R.; Mukherjeee, N. ZnO/Gamma-Fe_2O_3 Charge Transfer Interface toward Highly Selective H_2S Sensing at a Low Operating Temperature of 30 Degrees C. *Acs Sensors.* **2017,** *2*, 1831-1838.
(40) Zou, C. W.; Wang, J.; Xie, W. Synthesis and Enhanced NO_2 Gas Sensing Properties of ZnO Nanorods/TiO_2 Nanoparticles Heterojunction Composites. *J. Colloid Interface Sci.* **2016,** *478*, 22-28.
(41) Gao, X.; Sun, Y.; Zhu, C.; Li, C.; Ouyang, Q.; Chen, Y. Highly Sensitive and Selective H_2S Sensor Based on Porous $ZnFe_2O_4$ Nanosheets. *Sens. Actuators, B.* **2017,** *246*, 662-672.
(42) Liu, Z.; Fan, T.; Zhang, D.; Gong, X.; Xu, J. Hierarchically Porous ZnO with High Sensitivity and Selectivity to H_2S Derived from Biotemplates. *Sens. Actuators, B.* **2009,** *136*, 499-509.
(43) Shewale, P. S.; Agawane, G. L.; Shin, S. W.; Moholkar, A. V.; Lee, J. Y.; Kim, J. H.; Uplane, M. D. Thickness Dependent H_2S Sensing Properties of Nanocrystalline ZnO Thin Films Derived by Advanced Spray Pyrolysis. *Sens. Actuators, B.* **2013,** *177*, 695-702.
(44) Bulemo Peresi, M.; Cho, H.-J.; Kim, N.-H.; Kim, I.-D. Mesoporous SnO_2 Nanotubes Via Electrospinning-Etching Route: Highly Sensitive and Selective Detection of H_2S Molecule. *ACS Appl. Mater. Interfaces.* **2017,** *9*, 26304-26313.
(45) Pham Long, Q.; Nguyen Duc, C.; Tran Thai, H.; Hoang Thai, L.; Chu Manh, H.; Dang Thi Thanh, L.; Nguyen Van, H. Simple Post-Synthesis of Mesoporous P-Type Co_3O_4 Nanochains for Enhanced H_2S Gas Sensing Performance. *Sens. Actuators, B.* **2018,** *270*, 158-166.
(46) Ramgir Niranjan, S.; Datta, N.; Kumar, S.; Kailasaganapathi, S.; Patil, U. V.; Karmakar, N.; Kaur, M.; Debnath, A. K.; Kothari, D. C.; Aswal, D. K.; Gupta, S. K. Effect of Fe Modification on H_2S Sensing Properties of Rheotaxially Grown and Thermally Oxidized SnO_2 Thin Films. *Mater. Chem. Phys.* **2015,** *156*, 227-237.
(47) Bai, S.; Chen, C.; Zhang, D.; Luo, R.; Li, D.; Chen, A.; Liu, C.-C. Intrinsic Characteristic and Mechanism in Enhancing H_2S Sensing of Cd-Doped Alpha-MoO_3 Nanobelts. *Sens. Actuators, B.* **2014,** *204*, 754-762.
(48) Hosseini, Z. S.; Zad A, I.; Mortezaali, A. Room Temperature H_2S Gas Sensor Based on Rather Aligned ZnO Nanorods with Flower-Like Structures. *Sens. Actuators, B.* **2015,** *207*, 865-871.
(49) Zhang, B.; Li, M.; Song, Z.; Kan, H.; Yu, H.; Liu, Q.; Zhang, G.; Liu, H. Sensitive H_2S Gas Sensors Employing Colloidal Zinc Oxide Quantum Dots. *Sens. Actuators, B.* **2017,** *249*, 558-563.
(50) Kim, S.-J.; Na Chan, W.; Hwang, I.-S.; Lee, J.-H. One-Pot Hydrothermal Synthesis of CuO-ZnO Composite Hollow Spheres for Selective H_2S Detection. *Sens. Actuators, B.* **2012,** *168*, 83-89.
(51) Choi, S.-J.; Lee, I.; Jang, B.-H.; Youn, D.-Y.; Ryu, W.-H.; Park Chong, O.; Kim, I.-D. Selective Diagnosis of Diabetes Using Pt-Functionalized WO_3 Hemitube Networks as a Sensing Layer of Acetone in Exhaled Breath. *Anal. Chem.* **2013,** *85*, 1792-1796.
(52) Steinhauer, S.; Brunet, E.; Maier, T.; Mutinati, G. C.; Koeck, A. Suspended CuO Nanowires for Ppb Level H_2S Sensing in Dry and Humid Atmosphere. *Sens. Actuators, B.* **2013,** *186*, 550-556.
(53) Li, Z.; Wang, J.; Wang, N.; Yan, S.; Liu, W.; Fu Yong, Q.; Wang, Z. Hydrothermal Synthesis of Hierarchically Flower-Like CuO Nanostructures with Porous Nanosheets for Excellent H_2S Sensing. *J.*

Alloys Compd. **2017,** *725*, 1136-1143.
(54) Ayesh Ahmad, I.; Abu-Hani Ayah, F. S.; Mahmoud Saleh, T.; Haik, Y. Selective H_2S Sensor Based on CuO Nanoparticles Embedded in Organic Membranes. *Sens. Actuators, B.* **2016,** *231*, 593-600.
(55) Kim, H.; Jin, C.; Park, S.; Kim, S.; Lee, C. H_2S Gas Sensing Properties of Bare and Pd-Functionalized CuO Nanorods. *Sens. Actuators, B.* **2012,** *161*, 594-599.
(56) Zhang, S.; Zhang, P.; Wang, Y.; Ma, Y.; Zhong, J.; Sun, X. Facile Fabrication of a Well-Ordered Porous Cu-Doped SnO_2 Thin Film for H_2S Sensing. *ACS Appl. Mater. Interfaces.* **2014,** *6*, 14975-14980.
(57) Jagadale Tushar, C.; Prasad, V.; Ramgir Niranjan, S.; Prajapat, C.; Patil Uday, V.; Debnath, A.; Aswal, D. K.; Gupta, S. K. Greatly Enhanced H_2S Sensitivity Using Defect-Rich Titanium Oxide Films. *RSC Adv.* **2015,** *5*, 93081-93088.
(58) Wang, Y.; Qu, F.; Liu, J.; Wang, Y.; Zhou, J.; Ruan, S. Enhanced H_2S Sensing Characteristics of CuO-NiO Core-Shell Microspheres Sensors. *Sens. Actuators, B.* **2015,** *209*, 515-523.
(59) Guo, W.; Feng, Q.; Tao, Y.; Zheng, L.; Han, Z.; Ma, J. Systematic Investigation on the Gas-Sensing Performance of TiO_2 Nanoplate Sensors for Enhanced Detection on Toxic Gases. *Mater. Res. Bull.* **2016,** *73*, 302-307.
(60) Balouria, V.; Samanta, S.; Singh, A.; Debnath, A. K.; Mahajan, A.; Bedi, R. K.; Aswal, D. K.; Gupta, S. K. Chemiresistive Gas Sensing Properties of Nanocrystalline Co_3O_4 Thin Films. *Sens. Actuators, B.* **2013,** *176*, 38-45.
(61) Cai, J.; Goliney, I.; Philpott, M. R. Semiconductor-Metal Transition of Pyrite FeS_2 under High Pressure by Full-Potential Linearized-Augmented Plane Wave Calculations. *J. Phys.: Condens. Matter.* **2006,** *18*, 9151-9160.

Table of Contents